Arlon T. Adams (M'58–SM'72) received the B.A. degree in applied science from Harvard University, Cambridge, MA in 1953, and the M.S. and Ph.D. degrees in electrical engineering in 1961 and 1964, respectively, both from the University of Michigan, Ann Arbor.

He served as a Line Officer in the Atlantic Destroyer Fleet from 1953 to 1957, and until 1959, he was employed by Sperry Gyroscope Company, Long Island, NY. From 1959 to 1963, he was a Graduate Research Associate at the University of Michigan, Ann Arbor. In 1963, he joined the Faculty of Syracuse University, Syracuse, NY, where he is presently Professor of Electrical Engineering. During the academic year 1976–1977, he was a Visiting Scholar at the University of California at Berkeley where he worked on infrared antennas. His current interests are in numerical methods for electromagnetic problems. He is the author of a textbook on electromagnetic theory, coauthor of a textbook on electromagnetic compatibility, and has published over 70 papers on electromagnetics.

✤

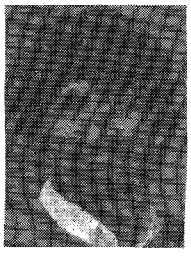

Yehuda Leviatan (S'81–M'82) was born in Jerusalem, Israel, on September 19, 1951. He received the B.Sc. and M.Sc. degrees in electrical engineering from the Technion-Israel Institute of Technology, Haifa, Israel, in 1977 and 1979, respectively, and the Ph.D. degree in electrical engineering from Syracuse University, Syracuse, NY, in 1982.

He held a Teaching Assistantship during his graduate work from 1977 to 1979 at the Technion, a Research Assistantship during his graduate work from 1979 to 1981 at Syracuse University, and a Postdoctoral Research position at Syracuse University during the summer of 1982. From 1980–1982, he was also engaged as a part-time Research Engineer at the Syracuse Research Corporation. In September 1982, he joined the Faculty of the Electrical and Computer Engineering Department at Syracuse University as an Assistant Professor. He provides consulting services to the Syracuse Research Corporation and to IBM. His research interests are in the areas of mathematical and numerical methods applied to antennas, transmission lines, and waveguides, scattering and transmission through apertures, near fields of radiating systems, and adaptive arrays.

✤

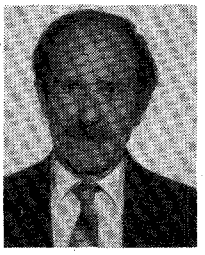

Jose Perini (M'61–SM'76) was born in São Paulo, Brazil. He received the B.S. degree in electrical and mechanical engineering from Escola Politecnica de São Paulo, São Paulo, Brazil, in 1952.

Subsequently, he worked for Real Transportes Aeroes, a Brazilian airline company, for three years, as Manager for Radio Maintenance, and in the last six months, as Assistant to the Manager of General Maintenance. In 1955, he joined the Electrical Engineering Department of Escola Politecnica de São Paulo, as an Assistant Professor, teaching until 1958. During this time, he also conducted ionospheric research. He received the Ph.D. degree in electrical engineering from Syracuse University, Syracuse, NY, in 1961. From 1959 to 1961, while studying at Syracuse, he was also a consultant for General Electric (G.E.) Co. in the Television Transmitting Antenna area. His Ph.D. dissertation was derived from this work. In 1961, he returned to Brazil as an Associate Professor of Electrical Engineering at Escola Politecnica de São Paulo and also as a consultant for G.E. of Brazil. In September 1962, he became Assistant Professor of Electrical Engineering at Syracuse University, where he was promoted to Associate Professor in 1966 and to Professor in 1971. He rejoined G.E. in Syracuse as a consultant in the same area of TV transmitting antennas until 1969. He has had many research contracts with the Navy, Air Force, and Army. He has consulted extensively in the U.S. and abroad in the areas of electromagnetics and communications. He has many published papers in the fields of antennas, microwaves, EMC, and circuit theory. He also holds two patents on TV transmitting antennas.

Theory and Numerical Modeling of a Compact Low-Field High-Frequency Gyrotron

PETER VITELLO, WILLIAM H. MINER, AND ADAM T. DROBOT

Abstract—**The electron-cyclotron maser interaction provides an extremely efficient means of generating high-power radiation in the millimeter and submillimeter regimes. For devices where both high frequencies and low magnetic fields are required, high cyclotron-harmonic interactions must be considered. We present here a linear and nonlinear analysis of a TE_{m11} whispering-gallery-mode gyrotron. Resonances at the mth and $(m \pm 1)$th cyclotron harmonic are found. The start oscillation condition is calculated from linear theory for a wide range of parameters. Maximum efficiency for different beam and cavity conditions is calculated with a fully relativistic numerical simulation code. High efficiencies, > 35 percent, have been found at the mth cyclotron harmonic. The effect on the efficiency of an initial velocity spread in the electron beam has also been considered.**

Manuscript received June 6, 1983; revised November 28, 1983. This work was supported in part by UCLA under Contract 400001 and in part by the U.S. Army Research Office, Triangle Research Park, NC, under Contract DAAG29-82-K-0004.

P. Vitello and A. Drobot are with Science Applications, Inc., McLean, VA 22102.

W. Miner is with the Fusion Research Center, University of Texas at Austin, Austin, TX 78712.

I. Introduction

THE ELECTRON-CYCLOTRON maser interaction provides perhaps one of the most efficient mechanisms for generating continuous high-power radiation in the millimeter and submillimeter regimes [1]–[6]. The interaction takes place between the electromagnetic (RF) waves of a cavity or waveguide, and an electron beam in which the electrons comprising the beam move along individual

0018-9480/84/0400-0373$01.00 ©1984 IEEE

helical orbits in the presence of an applied magnetic field, and is due to azimuthal bunching which results from the relativistic mass dependence on particle energy. The oscillation frequency is determined jointly by the cavity or waveguide and by the particle magnetic resonance. This allows the use of systems with higher mode densities than would be possible for most other devices, permitting cavity dimensions large compared to the radiation wavelength. Ohmic dissipation due to wall losses will be much smaller in such systems, and larger output powers are possible at a given frequency [7]. Research in the past decades has indicated that high-frequency radiation sources based upon the cyclotron maser mechanism may have great practical applications in areas ranging from RF heating of fusion plasmas [7]–[10] to new high-power short-wavelength radar systems [11] and plasma diagnostics.

Electron-cyclotron maser interaction studies have primarily addressed three types of devices, each representing a general experimental configuration. In the first [12]–[23], the traveling-wave amplifier, the interaction of the RF field with an electron beam leads to a spatial growth of the electromagnetic wave as it traverses the waveguide. In the second, the gyrotron oscillator [24]–[41], on which the present study is based, the electron beam interacts with a constant amplitude cavity standing-wave RF field. The third device is the quasioptical open-cavity resonator [42]–[46]. Operation at high frequencies at the fundamental cyclotron harmonic in each case requires background magnetic fields which only can be generated by superconducting magnets. At 100 GHz, for example, the required magnetic field would be $\simeq 35$ kg. In situations where high magnetic fields are not practical to achieve high frequencies, high cyclotron harmonics must be considered.

It is apparent that the most effective coupling to the high cyclotron harmonics for the cyclotron maser interaction occurs for the circular TE_{m11} (whispering-gallery) mode [3], [7], [34], [39]–[41], [47]. The TE_{m11} mode also is attractive in that it often suffers less mode competition than the TE_{on1} mode [7], and that the large-orbit electron beams needed are less affected by space charge [7]. Mode competition for TE_{m11} modes can be reduced further by the introduction of an azimuthal structure [39], [40], [48]. The TE_{m11} mode, however, does suffer from higher ohmic wall heating [7] (which is not significant for the output power levels considered in this paper) and from the need for a high-energy large-orbit electron beam for good high-harmonic operation due to the concentration of the RF field near to the cavity walls. Generation of the high-energy helical electron beam required can be efficiently accomplished, though, through the resonant acceleration of a low-energy beam in a cavity excited in the TE_{111} mode by an external high-power source of radiation [49]–[51].

The purpose of this paper is to present a fully relativistic linear and nonlinear analysis of the single-particle dynamics in a TE_{m11} gyrotron oscillator operating at the mth harmonic of the cyclotron frequency. The cavity configuration considered here is similar to that studied experimentally by Jory [47] and by McDermott *et al.* [51]. In a gyrotron, the nature of the cyclotron maser interaction is more complicated than in a traveling-wave amplifier [34], mainly due to the RF wave now consisting of both a forward and a backward wave. The gyrotron is, therefore, much more difficult to model analytically in the nonlinear regime. We have for this reason, in the present analysis, limited our analytic treatment primarily to the weak-field regime. For large RF fields, where the behavior is nonlinear, we have used a numerical treatment of the particle dynamics. The linear model provides a parameterization of the start oscillation condition, and an understanding of the instability mechanism. The linear theory also provides a useful check of the nonlinear code at low-field amplitudes.

In the nonlinear regime, we find that the primary mechanism for saturation of the efficiency is due to phase trapping. The trapping width is determined by both the external magnetic field and the amplitude of the RF field in the cavity. We have studied the effect on interaction efficiency due to m-mode number, cavity dimensions, beam energy, pitch angle, beam velocity spread, and beam position. We find that efficiencies > 35 percent can be achieved in simple cavities without resorting to magnetic field shaping or complicated cavity design.

This paper is organized as follows. In Section II, we present the model used along with the basic equations and assumptions. In Section III, an analytic treatment of the linear regime is presented and start oscillation currents are derived. Section IV consists of a nonlinear numerical analysis of the gyrotron system. Conclusions are presented in Section V.

II. Model, Basic Equations, and Assumptions

In the TE_{m11} whispering-gallery-mode gyrotron under study, a large helical-orbit axis-encircling electron beam is injected into an open-ended cylindrical cavity and propagates along the z axis, guided by a magnetic field (Fig. 1). We have considered the beam as being initially cold and monoenergetic. The electron beams treated are typical of those generated by a TE_{111} resonant accelerator cavity [49], [50], and have kinetic energy predominantly transverse to the direction of the axial guide magnetic field. This is highly desirable for the cyclotron maser interaction, which, under optimum conditions, leads to azimuthal electron bunching, with a subsequent loss of transverse kinetic energy to the RF fields. Electrons with initial energies in the range of 50–300 keV are considered. We assume in this paper that, for the moderate-output power levels considered, the beam is sufficiently tenuous that space charge fields can be neglected, and that the beam does not modify the normal-mode RF field structure of the cavity. The cavity modes used are those for closed cavities, neglecting the beam input and output apertures. In a subsequent paper, we will consider space-charge effects and cavity modes, including the effects of finite apertures. A single standing-mode approximation was used in the analysis. As an additional approximation, the tightly wound spiral of the beam was treated as a hollow rotating shell of charge.

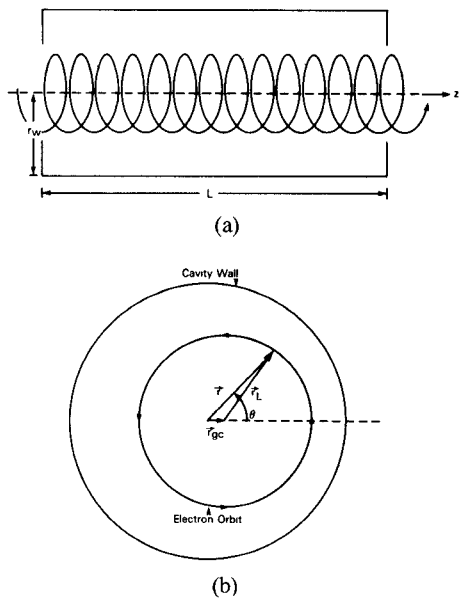

Fig. 1. (a) Side view and (b) end view of the gyrotron oscillator. The three vectors $\vec{r}$, $\vec{r}_{gc}$, and $\vec{r}_L$ give the electron's radial position, the center of its orbit relative to the cavity center, and its Larmor radius about this guiding center.

Under our assumptions, the relativistic electron equation of motions is

$$\frac{d\vec{U}}{dt} = -\frac{|e|}{m_e}\left(\vec{E} + \frac{\vec{U}\times\vec{B}}{\gamma}\right) \tag{1}$$

where $\vec{U}$ is the electron four-velocity, e is the electron charge, m_e is the electron rest mass, $\gamma = (1+U^2/c^2)^{1/2}$ is the Lorentz factor, c is the speed of light, $\vec{E} = (E_r, E_\theta, 0)$, $\vec{B} = (B_r, B_\theta, B_0 + B_z)$, B_0 is the applied background magnetic field, and E_r, E_θ, B_r, B_θ, and B_z are the TE_{mnl} RF circularly polarized standing-wave fields given by

$$E_r = -E_0\left(\frac{mJ_m(k_\perp r)}{k_\perp r}\right)\sin(k_\parallel z)\cos(m\theta - \omega t) \tag{2}$$

$$E_\theta = E_0 J_m'(k_\perp r)\sin(k_\parallel z)\sin(m\theta - \omega t) \tag{3}$$

$$B_r = E_0\left(\frac{ck_\parallel}{\omega}\right)J_m'(k_\perp r)\cos(k_\parallel z)\cos(m\theta - \omega t) \tag{4}$$

$$B_\theta = -E_0\left(\frac{ck_\parallel}{\omega}\right)\left(\frac{mJ_m(k_\perp r)}{k_\perp r}\right)\cos(k_\parallel z)\sin(m\theta - \omega t) \tag{5}$$

and

$$B_z = E_0\left(\frac{ck_\perp}{\omega}\right)J_m(k_\perp r)\sin(k_\parallel z)\cos(m\theta - \omega t). \tag{6}$$

In (2)–(6), a prime indicates differentiation with respect to the arguments, $k_\perp = x_{mn}/r_w$, where x_{mn} is the nth nonvanishing root of $J_m'(x) = 0$, $J_m(x)$ is the well-known Bessel function, r_w is the cavity radius, $k_\parallel = \pi l/L$, where L is the cavity length, and $\omega = c(k_\perp^2 + k_\parallel^2)^{1/2}$ is the wave frequency. We have, for the most part, considered cavities for which $\omega \simeq k_\perp c$ and where $k_\perp \gg k_\parallel$ so that the RF magnetic field components B_r and B_θ are small compared to E_r and E_θ. These TE_{mnl} modes are fast waves, and this fact will be exploited in the analysis. The electron positions can be followed by solving

$$\frac{d\vec{x}}{dt} = \frac{\vec{U}}{\gamma}. \tag{7}$$

The equation for the particle energy γ can be obtained from (1), to give

$$\frac{d\gamma}{dt} = -\frac{|e|\vec{U}\cdot\vec{E}}{\gamma m_e c^2}. \tag{8}$$

Circular polarization only was considered. The results for a linearly polarized standing wave for the cases studied are essentially the same as for a circularly polarized wave of half its amplitude. The component of the linear wave with rotational direction opposite to the beam averages out. For convenience, we switch now to dimensionless units, using the cavity radius as our scaling parameter. In the new units (normalized notation will be denoted by a bar), length is measured in units of r_w, time in units of r_w/c, and fields in units of $m_e c^2/|e|r_w$. This allows us to rewrite (1)–(8) as

$$\frac{d\vec{\bar{U}}}{dt} = -\left(\vec{\bar{E}} + \frac{\vec{\bar{U}}\times\vec{\bar{B}}}{\gamma}\right) \tag{9}$$

$$\bar{E}_r = -\bar{E}_0\left(\frac{mJ_m(\bar{k}_\perp \bar{r})}{\bar{k}_\perp \bar{r}}\right)\sin(\bar{k}_\parallel \bar{z})\cos(m\theta - \overline{\omega t}) \tag{10}$$

$$\bar{E}_\theta = \bar{E}_0 J_m'(\bar{k}_\perp \bar{r})\sin(\bar{k}_\parallel \bar{z})\sin(m\theta - \overline{\omega t}) \tag{11}$$

$$\bar{B}_r = \bar{E}_0\left(\frac{\bar{k}_\parallel}{\bar{\omega}}\right)J_m'(\bar{k}_\perp \bar{r})\cos(\bar{k}_\parallel \bar{r})\cos(m\theta - \overline{\omega t}) \tag{12}$$

$$\bar{B}_\theta = -\bar{E}_0\left(\frac{\bar{k}_\parallel}{\bar{\omega}}\right)\left(\frac{mJ_m(\bar{k}_\perp \bar{r})}{\bar{k}_\perp \bar{r}}\right)\cos(\bar{k}_\parallel \bar{z})\sin(m\theta - \overline{\omega t}) \tag{13}$$

$$\bar{B}_z = \bar{E}_0\left(\frac{\bar{k}_\perp}{\bar{\omega}}\right)J_m(\bar{k}_\perp \bar{r})\sin(\bar{k}_\parallel \bar{z})\cos(m\theta - \overline{\omega t}) \tag{14}$$

$$\frac{d\vec{\bar{x}}}{d\bar{t}} = \frac{\vec{\bar{U}}}{\gamma} \tag{15}$$

and

$$\frac{d\gamma}{d\bar{t}} = -\frac{\vec{\bar{U}}\cdot\vec{\bar{E}}}{\gamma}. \tag{16}$$

In our analysis, we have considered the whispering-gallery gyrotron system to be in steady state, with the power output (P_w) due to diffractive loss (assuming negligible wall heating) balancing the energy loss of the beam power (P_b) to the cavity fields. The wave energy stored in the cavity can be written as

$$W_f = 0.25\pi\epsilon_0 E_0^2 L r_w^2 J_m^2(x_{mn})(1 - m^2/x_{mn}^2). \tag{17}$$

This leads, for a give cavity Q factor, to

$$\begin{aligned} P_w &= \omega W_f/Q \\ &= 0.25\pi\epsilon_0\omega E_0^2 L r_w^2 J_m^2(x_{mn})(1 - m^2/x_{mn}^2)/Q \\ &= 5.4\times 10^5 \bar{\omega}\bar{E}_0^2\bar{L}J_m^2(x_{mn})(1 - m^2/x_{mn}^2)/Q\ \text{kW}. \end{aligned} \tag{18}$$

The beam energy to sustain the steady-state fields is given by

$$P_b = IV_0 = P_w/\eta = \frac{5.4\times10^5\bar{\omega}\bar{E}_0^2\bar{L}J_m^2(x_{mn})(1-m^2/x_{mn}^2)}{Q\eta}\,kW \quad (19)$$

where I is the beam current, V_0 is the initial beam energy in volts, and where η is the efficiency defined as the ratio of the loss in beam electron kinetic energy to its initial kinetic energy

$$\eta = \left(\frac{\gamma_0-\gamma_f}{\gamma_0-1}\right). \quad (20)$$

In (20), γ_0 and γ_f are, respectively, the average initial and final values for the beam γ. The efficiency η is the quantity to be solved for in terms of the beam, cavity, and field parameters, in order to determine the gyrotron power balance. Defining the guiding center radius $\bar{r}_{gc}$, about which the cylindrical shell beam is initially centered, the parameters of the system are: $\bar{r}_{gc}$, $\beta_{\|0}$, $\beta_{\perp 0}$, $\bar{L}$, $\bar{E}_0$, $\bar{B}_0$, m, n, and l, where $\beta_{\|0}=\bar{U}_{z0}/\gamma_0$ and $\beta_{\perp 0}=\bar{U}_{\perp 0}/\gamma_0$ are the initial parallel and perpendicular velocities normalized to the speed of light, and $\bar{U}_{\perp 0}=(\bar{U}_{r0}^2+\bar{U}_{\theta 0}^2)^{1/2}$.

Our primary interest in this paper is the cyclotron maser interaction, which, for a TE_{mnl} mode and an axis-encircling electron beam, occurs at the mth cyclotron harmonic for angular frequencies

$$\omega \geq \frac{m\Omega}{\gamma_0} \quad (21)$$

where Ω is the rest-mass cyclotron frequency

$$\Omega = \frac{|e|B_0}{m_e c}. \quad (22)$$

(Note that, in dimensionless units, (21) and (22) give $\bar{\omega}\geq m\bar{\Omega}/\gamma_0 = m\bar{B}_0/\gamma_0$.) For magnetic fields satisfying relation (21), there are strong limitations on the orbital position of the beam. Ignoring the magnetic field associated with the RF radiation, the electron Larmor radius is

$$\bar{r}_L = \frac{\bar{U}_\perp}{\bar{B}_0}. \quad (23)$$

When $\bar{\omega}\geq m\bar{\Omega}/\gamma$, $\bar{r}_L$ satisfies the inequality

$$\bar{r}_L \geq \frac{m\beta_\perp}{x_{mn}} \quad (24)$$

where we assume $\bar{\omega}\gg\bar{k}_\|$. The RF electric field has its maximum near to the wall. Unless $\beta_\perp\simeq 1$ (i.e., a high-energy beam), the electron orbit lies well within the radial peak of the RF field and the interaction is poor. For $n>1$, orbits lie within the first radial maxima as the relation for the Bessel function argument $\bar{k}_\perp\bar{r}_L\geq m\beta_\perp$ is independent of n.

III. Linear Regime

We present here a treatment of the weak RF field regime for which the particle dynamics can be handled by linear theory. We have solved the single-particle equations (9)–(15) in place of the linearized Vlasov equation in order to facilitate direct comparison with the numerical nonlinear high-field treatment, which uses the same equations. In our fully relativistic linear perturbation treatment, all RF field components are retained, and the approximations for $\bar{\omega}\gg\bar{k}_\|$ and $\beta_{\|0}\ll 1$ are made only at the end. Resonances were found for $\bar{\omega}\simeq m\bar{\Omega}/\gamma_0$, and $\bar{\omega}\simeq(m\pm1)\bar{\Omega}/\gamma_0$. The $(m+1)$th harmonic interaction leads to absorption, the mth harmonic interaction allows both emission and absorption and the $(m-1)$th harmonic leads to emission. The $(m\pm1)$th harmonics are often missing from the analysis in some of the existing literature because of approximations that do not consider the radial displacement of the large-orbit beam, but concentrate on azimuthal variations that do lead correctly to solutions for the mth harmonic cyclotron maser interaction. We consider here, primarily, the $\bar{\omega}\simeq m\bar{\Omega}/\gamma_0$ resonance, which is caused by the relativistic cyclotron maser instability. We leave the $(m-1)$th harmonic emission, which comes from a nonrelativistic radial instability, to a subsequent investigation (see Sprangle [16] for a discussion of these three modes for a traveling-wave amplifier). The $(m-1)$th interaction corresponds to the Peniotron [52].

In treating the weak-field particle orbits, we make here a change of variables, replacing $(\bar{U}_r,\bar{U}_\theta)$ by $(\bar{U}_\perp,\Lambda)$, where

$$\bar{U}_\theta = \bar{U}_\perp\sin(\Lambda) \quad (25)$$

and

$$\bar{U}_r = \bar{U}_\perp\cos(\Lambda). \quad (26)$$

In terms of these new variables, the momentum and position equations (9) and (15), become

$$\frac{d\bar{U}_z}{d\bar{t}} = -\frac{\bar{U}_\perp}{\gamma}\left(\cos(\Lambda)\bar{B}_\theta - \sin(\Lambda)\bar{B}_r\right) \quad (27)$$

$$\frac{d\bar{U}_\perp}{d\bar{t}} = -\left[\left(\bar{E}_\theta+\frac{\bar{U}_z}{\gamma}\bar{B}_r\right)\sin(\Lambda) + \left(\bar{E}_r-\frac{\bar{U}_z}{\gamma}\bar{B}_\theta\right)\cos(\Lambda)\right] \quad (28)$$

$$\frac{d\Lambda}{d\bar{t}} = -\frac{1}{\bar{U}_\perp}\left[\left(\bar{E}_\theta+\frac{\bar{U}_z\bar{B}_r}{\gamma}\right)\cos(\Lambda) - \left(\bar{E}_r-\frac{\bar{U}_z\bar{B}_\theta}{\gamma}\right)\sin(\Lambda)\right] + \frac{1}{\gamma}\left(\bar{B}_0+\bar{B}_z-\frac{\bar{U}_\perp}{\bar{r}}\sin(\Lambda)\right) \quad (29)$$

$$\frac{d\bar{z}}{d\bar{t}} = \frac{\bar{U}_z}{\gamma} \quad (30)$$

$$\frac{d\theta}{d\bar{t}} = \frac{\bar{U}_\perp\sin(\Lambda)}{\gamma\bar{r}} \quad (31)$$

and

$$\frac{d\bar{r}}{d\bar{t}} = \frac{\bar{U}_\perp\cos(\Lambda)}{\gamma}. \quad (32)$$

The zero-order orbits for axis-encircling electrons with initial velocities $\bar{U}_{z0}$ and $\bar{U}_{\perp 0}$ in the absence RF fields have

as their solution

$$\bar{U}_z = \bar{U}_{z0} \tag{33a}$$

$$\bar{U}_\perp = \bar{U}_{\perp 0} \tag{33b}$$

$$\Lambda = \pi/2 \tag{33c}$$

$$\bar{z} = \frac{\bar{U}_{z0}}{\gamma_0}\bar{t} \tag{33d}$$

$$\bar{r} = \bar{r}_0 = \frac{\bar{U}_{\perp 0}}{\bar{B}_0} = \frac{\bar{U}_{\perp 0}}{\bar{\Omega}} \tag{33e}$$

and

$$\theta = \theta_0 + \frac{\bar{\Omega}}{\gamma_0}\bar{t} \tag{33f}$$

where we have taken $\bar{z} = 0$, and $\theta = \theta_0$ at $\bar{t} = 0$.

Using (33), we linearize (27)–(32), using $\bar{E}_0$ as our small expansion parameter, to obtain the equations for the perturbed velocities and positions

$$\frac{d\delta\bar{U}_z}{d\bar{t}} = \frac{\bar{U}_{\perp 0}}{\gamma_0}\bar{B}_r \tag{34}$$

$$\frac{d\delta\bar{U}_\perp}{d\bar{t}} = -\left(\bar{E}_\theta + \frac{\bar{U}_{z0}}{\gamma_0}\bar{B}_r\right) \tag{35}$$

$$\frac{d\delta\Lambda}{d\bar{t}} = \frac{1}{\bar{U}_{\perp 0}}\left(\bar{E}_r - \frac{\bar{U}_{z0}}{\gamma_0}\bar{B}_\theta\right) + \frac{1}{\gamma_0}\left(\bar{B}_z - \frac{\Omega\delta\bar{U}_\perp}{\bar{U}_{\perp 0}} + \frac{\bar{\Omega}\delta\bar{r}}{\bar{r}_0}\right) \tag{36}$$

$$\frac{d\delta\bar{z}}{d\bar{t}} = \frac{1}{\gamma_0^3}\left[\gamma_{\perp 0}^2\delta\bar{U}_z - \bar{U}_{z0}\bar{U}_{\perp 0}\delta\bar{U}_\perp\right] \tag{37}$$

$$\frac{d\delta\theta}{d\bar{t}} = \frac{\bar{\Omega}}{\gamma_0}\left(\frac{\gamma_{z0}^2\delta\bar{U}_\perp}{\gamma_0^2\bar{U}_{\perp 0}} - \frac{\delta\bar{r}}{\bar{r}_0} - \frac{\bar{U}_{z0}\delta\bar{U}_z}{\gamma_0^2}\right) \tag{38}$$

and

$$\frac{d\delta\bar{r}}{d\bar{t}} = -\frac{\bar{U}_{\perp 0}}{\gamma_0}\delta\Lambda \tag{39}$$

where $\gamma_{\perp 0}^2 = 1 + \bar{U}_{\perp 0}^2$ and $\gamma_{z0}^2 = 1 + \bar{U}_{z0}^2$. (Note that $\delta U_r = -\bar{U}_{\perp 0}\delta\Lambda$.)

Using the RF fields given in (10)–(14), we integrate for $\delta\bar{U}_z$ and $\delta\bar{U}_\perp$ along the unperturbed orbits, to find

$$\delta\bar{U}_z = \left(\frac{\bar{E}_0}{2}\right)(J_m')\left(\frac{\bar{k}_\parallel\bar{U}_{\perp 0}}{\bar{\omega}\gamma_0}\right) \cdot\left\{\frac{[\sin(m\theta_0 + \psi^+\bar{t}) - \sin(m\theta_0)]}{\psi^+} + \frac{[\sin(m\theta_0 + \psi^-\bar{t}) - \sin(m\theta_0)]}{\psi^-}\right\} \tag{40}$$

$$\delta\bar{U}_\perp = \left(\frac{\bar{E}_0}{2}\right)(J_m')\left\{\left[1 - \frac{\bar{k}_\parallel\bar{U}_{z0}}{\bar{\omega}\gamma_0}\right] \cdot\frac{[\sin(m\theta_0 + \psi^+\bar{t}) - \sin(m\theta_0)]}{\psi^+} - \left[1 + \frac{\bar{k}_\parallel\bar{U}_{z0}}{\bar{\omega}\gamma_0}\right]\frac{[\sin(m\theta_0 + \psi^-\bar{t}) - \sin(m\theta_0)]}{\psi^-}\right\} \tag{41}$$

where $\psi^\pm = \pm\bar{k}_\parallel\bar{U}_{z0}/\gamma_0 + m\bar{\Omega}/\gamma_0 - \bar{\omega}$, and the argument of the Bessel functions is $\bar{k}_\perp\bar{r}_0$. $\psi^\pm = 0$ gives the mth harmonic resonance conditions with the forward and backward RF wave, respectively. When $l = 1$, the forward and backward waves cross-couple strongly. For $l > 1$, two separate resonances arise.[11] For interactions under fast-wave conditions, when $\bar{k}_\parallel \ll \bar{\omega}$, we find $|\delta\bar{U}_z| \ll |\delta\bar{U}_\perp|$.

Equation (36) for $\delta\Lambda$ cannot be integrated directly, as it contains $\delta\bar{r}$. However, taking its derivative with respect to time and using (39) gives a second-order inhomogeneous equation for $\delta\Lambda$ which can then be solved to yield

$$\delta\Lambda = \left(\frac{\bar{E}_0}{2\bar{U}_{\perp 0}}\right)\left\{\frac{\gamma_0}{\bar{\Omega}}\left[2\left(\frac{\bar{k}_\parallel\bar{U}_{z0}}{\bar{\omega}\gamma_0}\right)\left(\frac{mJ_m}{\bar{k}_\perp\bar{r}_0}\right) + \left(\psi^+ - \frac{\bar{\Omega}}{\gamma_0}\right)A + \left(\psi^- - \frac{\bar{\Omega}}{\gamma_0}\right)B\right]\sin(m\theta_0)\sin\left(\frac{\bar{\Omega}}{\gamma_0}\bar{t}\right) + A\left[\cos(m\theta_0 + \psi^+\bar{t}) - \cos\left(m\theta_0 + \frac{\bar{\Omega}}{\gamma_0}\bar{t}\right)\right] + B\left[\cos(m\theta_0 + \psi^-\bar{t}) - \cos\left(m\theta_0 + \frac{\bar{\Omega}}{\gamma_0}\bar{t}\right)\right]\right\} \tag{42}$$

where

$$A = -\frac{\left\{\left[1 - \frac{\bar{k}_\parallel\bar{U}_{z0}}{\bar{\omega}\gamma_0}\right]\left[\psi^+\left(\frac{mJ_m}{\bar{k}_\perp\bar{r}_0}\right) + \frac{\bar{\Omega}}{\gamma_0}(J_m')\right] - \left[\frac{\bar{k}_\perp\bar{U}_{\perp 0}}{\gamma_0\bar{\omega}}\right]\psi^+ J_m\right\}}{\left\{\left[\frac{\bar{\Omega}}{\gamma_0}\right]^2 - [\psi^+]^2\right\}} \tag{43}$$

and

$$B = \frac{\left\{\left[1 + \frac{\bar{k}_\parallel\bar{U}_{z0}}{\bar{\omega}\gamma_0}\right]\left[\psi^-\left(\frac{mJ_m}{\bar{k}_\perp\bar{r}_0}\right) + \frac{\bar{\Omega}}{\gamma_0}(J_m')\right] - \left[\frac{\bar{k}_\perp\bar{U}_{\perp 0}}{\gamma_0\bar{\omega}}\right]\psi^- J_m\right\}}{\left\{\left[\frac{\bar{\Omega}}{\gamma_0}\right]^2 - [\psi^-]^2\right\}}. \tag{44}$$

Near the mth harmonic resonance (i.e., where $|\psi^+|, |\psi^-| \ll \bar{\Omega}/\gamma_0$), $\delta\Lambda$ can be approximated, for $\bar{\omega} \gg \bar{k}_\parallel U_{z0}/\gamma_0$, as

$$\delta\Lambda \simeq -\left(\frac{\bar{E}_0}{2\bar{U}_{\perp 0}}\right)\left(\frac{\gamma_0}{\bar{\Omega}}\right)(J_m')[\cos(m\theta_0 + \psi^+\bar{t}) - \cos(m\theta_0 + \psi^-\bar{t})]. \tag{45}$$

This resulting value for $\delta\Lambda$ comes from the centrifugal force term in (36).

Equations (37) and (38) now can be integrated to give

$$\delta\bar{z} = \left(\frac{\bar{U}_{\perp 0}\bar{E}_0}{2\gamma_0^2}\right)(J_m')\left\{\left[\frac{\bar{U}_{z0}}{\gamma_0} - \frac{\bar{k}_{\parallel}}{\bar{\omega}}\right]\left[\frac{[\cos(m\theta_0 + \psi^+\bar{t}) - \cos(m\theta_0)]}{(\psi^+)^2} + \frac{\bar{t}\sin(m\theta_0)}{\psi^+}\right] - \left[\frac{\bar{U}_{z0}}{\gamma_0} + \frac{\bar{k}_{\parallel}}{\bar{\omega}}\right]\left[\frac{[\cos(m\theta_0 + \psi^-\bar{t}) - \cos(m\theta_0)]}{(\psi^-)^2} + \frac{\bar{t}\sin(m\theta_0)}{\psi^-}\right]\right\} \quad (46)$$

$$\delta\theta = \left(\frac{\bar{E}_0}{2\bar{U}_{\perp 0}}\right)\left\{G\left[\frac{[\cos(m\theta_0 + \psi^+\bar{t}) - \cos(m\theta_0)]}{(\psi^+)^2} + \frac{\bar{t}\sin(m\theta_0)}{\psi^+}\right] + H\left[\frac{[\cos(m\theta_0 + \psi^-\bar{t}) - \cos(m\theta_0)]}{(\psi^-)^2} + \frac{\bar{t}\sin(m\theta_0)}{\psi^-}\right] + I\left[\frac{\left[\cos\left(m\theta_0 + \frac{\bar{\Omega}}{\gamma_0}\bar{t}\right) - \cos(m\theta_0)\right]}{\left(\frac{\bar{\Omega}}{\gamma_0}\right)^2} + \frac{\bar{t}\sin(m\theta_0)}{\frac{\bar{\Omega}}{\gamma_0}}\right] + J\left[\frac{\sin\left(\frac{\bar{\Omega}}{\gamma_0}\bar{t}\right)}{\frac{\bar{\Omega}}{\gamma_0}} - \bar{t}\right]\sin(m\theta_0)\right\} \quad (47)$$

and

$$\delta\bar{r} = \left(\frac{\bar{E}_0}{2\gamma_0}\right)\left\{\left(\frac{\gamma_0}{\bar{\Omega}}\right)^2\left[\left[2\left(\frac{\bar{k}_{\parallel}\bar{U}_{z0}}{\bar{\omega}\gamma_0}\right)\left(\frac{mJ_m}{\bar{k}_{\perp}\bar{r}_0}\right) + \left(\psi^+ - \frac{\bar{\Omega}}{\gamma_0}\right)A + \left(\psi^- - \frac{\bar{\Omega}}{\gamma_0}\right)B\right]\cdot\sin(m\theta_0)\left[\cos\left(\frac{\bar{\Omega}}{\gamma_0}\bar{t}\right) - 1\right]\right] - A\left[\frac{[\sin(m\theta_0 + \psi^+\bar{t}) - \sin(m\theta_0)]}{\psi^+} - \frac{\left[\sin\left(m\theta_0 + \frac{\bar{\Omega}}{\gamma_0}\bar{t}\right) - \sin(m\theta_0)\right]}{\frac{\bar{\Omega}}{\gamma_0}}\right] - B\left[\frac{[\sin(m\theta_0 + \psi^-\bar{t}) - \sin(m\theta_0)]}{\psi^-} - \frac{\left[\sin\left(m\theta_0 + \frac{\bar{\Omega}}{\gamma_0}\bar{t}\right) - \sin(m\theta_0)\right]}{\frac{\bar{\Omega}}{\gamma_0}}\right]\right\} \quad (48)$$

where

$$G = -(J_m')\left[\frac{\bar{\Omega}}{\gamma_0}\left(\frac{\gamma_{z0}^2}{\gamma_0^2} - \frac{\bar{k}_{\parallel}\bar{U}_{z0}}{\bar{\omega}\gamma_0}\right)\right] - \left(\frac{\bar{\Omega}}{\gamma_0}\right)^2 A \quad (49)$$

$$H = (J_m')\left[\frac{\bar{\Omega}}{\gamma_0}\left(\frac{\gamma_{z0}^2}{\gamma_0^2} + \frac{\bar{k}_{\parallel}\bar{U}_{z0}}{\bar{\omega}\gamma_0}\right)\right] - \left(\frac{\bar{\Omega}}{\gamma_0}\right)^2 B \quad (50)$$

$$I = \left(\frac{\bar{\Omega}}{\gamma_0}\right)^2 (A + B) \quad (51)$$

and

$$J = -\left[2\left(\frac{\bar{k}_{\parallel}\bar{U}_{z0}}{\bar{\omega}\gamma_0}\right)\left(\frac{mJ_m}{\bar{k}_{\perp}\bar{r}_0}\right) + \left(\psi^+ - \frac{\bar{\Omega}}{\gamma_0}\right)A + \left(\psi^- - \frac{\bar{\Omega}}{\gamma_0}\right)B\right]. \quad (52)$$

The $(m+1)$th, mth, and $(m-1)$th harmonic resonances are apparent in the relations for $\delta\Lambda$, $\delta\bar{r}$, and $\delta\theta$. For fast-wave interactions near the mth harmonic with $\bar{U}_{z0}/\gamma_0$

$\ll 1$, the expressions for $\delta\theta$ and $\delta\bar{r}$ can be reduced to

$$\delta\theta \simeq \left(\frac{\bar{U}_{\perp 0}\bar{E}_0}{2\gamma_0^2}\right)(J_m')\left(\frac{\bar{\Omega}}{\gamma_0}\right) \cdot\left[\left[\frac{\cos(m\theta_0+\psi^+\bar{t})-\cos(m\theta_0)}{(\psi^+)^2}+\frac{\bar{t}\sin(m\theta_0)}{\psi^+}\right] -\left[\frac{\cos(m\theta_0+\psi^-\bar{t})-\cos(m\theta_0)}{(\psi^-)^2}+\frac{\bar{t}\sin(m\theta_0)}{\psi^-}\right]\right] \tag{53}$$

and

$$\delta\bar{r} \simeq \left(\frac{\bar{E}_0}{2}\right)(J_m')\left(\frac{1}{\bar{\Omega}}\right)\left[\left[\frac{\sin(m\theta_0+\psi^+\bar{t})-\sin(m\theta_0)}{\psi^+}\right] -\left[\frac{\sin(m\theta_0+\psi^-\bar{t})-\sin(m\theta_0)}{\psi^-}\right]\right]. \tag{54}$$

On comparing $\delta\bar{r}$ and $\delta\bar{U}_\perp$ from (54) and (41), we see that $\delta\bar{r}/\bar{r}_0 \simeq \delta\bar{U}_\perp/\bar{U}_{\perp 0}$, which implies that the electron orbits remain nearly centered on the axis. The resultant perturbation in $\delta\theta$ in (53) comes from the relativistic variation in the cyclotron frequency. This is most evident from comparing (53) for $\delta\theta$ and (41) for $\delta\bar{U}_\perp$ which shows that azimuthal bunching is due to a variation in γ as indicated in the following equation:

$$\frac{d}{d\bar{t}}\delta\theta \simeq -\frac{\bar{\Omega}}{\gamma_0^2}\delta\gamma. \tag{55}$$

To calculate the average change in kinetic energy for our cylindrical beam, we solve for the perturbed Lorentz factor $\delta\gamma$ by using (16) and averaging over the initial phase θ_0. Upon linearization, (16) becomes

$$\frac{d\delta\gamma}{d\bar{t}} = -\frac{\bar{U}_{\perp 0}}{\gamma_0}\left(\frac{\gamma_{z0}^2\delta\bar{U}_\perp}{\gamma_0^2\bar{U}_{\perp 0}}-\frac{\bar{U}_{z0}\delta\bar{U}_{z0}}{\gamma_0^2}\right)\bar{E}_\theta+\frac{\bar{U}_{\perp 0}}{\gamma_0}(\delta\Lambda)\bar{E}_r -\frac{\bar{U}_{\perp 0}}{\gamma_0}\left(\delta\bar{z}\frac{\partial\bar{E}_\theta}{\partial\bar{z}}\right)-\frac{\bar{U}_{\perp 0}}{\gamma_0}\left(\delta\theta\frac{\partial\bar{E}_\theta}{\partial\theta}\right)-\frac{\bar{U}_{\perp 0}}{\gamma_0}\left(\delta\bar{r}\frac{\partial\bar{E}_0}{\partial\bar{r}}\right) \tag{56}$$

where we have made use of the initial condition $\bar{U}_{r0}=0$, which corresponds to that of an axis-encircling beam. The terms in this equation come from the variation of $\bar{U}_\theta/\gamma$, $\bar{U}_r/\gamma$, $\delta\bar{z}$, $\delta\theta$, and $\delta\bar{r}$, respectively, and assume a TE mode. Equation (56) is integrated along the unperturbed orbit from $\bar{t}=0$ to $\bar{t}=\bar{L}\gamma_0/\bar{U}_{z0}$. The resulting solution for $\delta\gamma$ is partitioned into five components, which come from the respective five terms in (56)

$$\delta\gamma = \left[\frac{\bar{E}_0\gamma_0}{\bar{k}_\parallel\bar{U}_{z0}}\right]^2(a_1+a_2+a_3+a_4+a_5) \tag{57}$$

where

$$a_1 = \left(\frac{1}{\gamma_0}\right)(J_m')^2\left(\frac{m\bar{\Omega}}{\bar{\omega}\gamma_0}-\frac{\bar{U}_{\perp 0}^2}{\gamma_0^2}\right)g(x) \tag{58}$$

$$a_2 = \left(\frac{1}{4\gamma_0}\right)\left(\frac{mJ_m}{\bar{k}_\perp\bar{r}_0}\right)\left(\frac{\bar{k}_\parallel\bar{U}_{z0}}{\gamma_0}\right)^2\left(\frac{\gamma_0}{\bar{\Omega}}\right)\left\{\left[\frac{2}{\bar{\omega}}\left(\frac{mJ_m}{\bar{k}_\perp\bar{r}_0}\right) +\left(\frac{\gamma_0}{\bar{k}_\parallel\bar{U}_{z0}}\right)\left(\psi^+-\frac{\bar{\Omega}}{\gamma_0}\right)A+\left(\frac{\gamma_0}{\bar{k}_\parallel\bar{U}_{z0}}\right)\left(\psi^--\frac{\bar{\Omega}}{\gamma_0}\right)B\right]h(x^+) -\left[\frac{2}{\bar{\omega}}\left(\frac{mJ_m}{\bar{k}_\perp\bar{r}_0}\right)+\left(\frac{\gamma_0}{\bar{k}_\parallel\bar{U}_{z0}}\right)\left(\psi^++\frac{\bar{\Omega}}{\gamma_0}\right)A +\left(\frac{\gamma_0}{\bar{k}_\parallel\bar{U}_{z0}}\right)\left(\psi^-+\frac{\bar{\Omega}}{\gamma_0}\right)B\right]h(x^-)\right\} \tag{59}$$

$$a_3 = \left(\frac{U_{\perp 0}^2}{\gamma_0^3}\right)(J_m')^2\left\{x\left[1+x\left(\frac{\gamma_0}{\bar{U}_{z0}}\right)\left(\frac{k_\parallel}{\bar{\omega}}\right)\right]g'(x) +\left[1+2x\left(\frac{\gamma_0}{\bar{U}_{z0}}\right)\left(\frac{k_\parallel}{\bar{\omega}}\right)\right]g(x)\right\} \tag{60}$$

$$a_4 = \left(\frac{m}{4\gamma_0}\right)(J_m')\left\{2\left(\frac{\gamma_0}{\bar{k}_\parallel\bar{U}_{z0}}\right)[G(g(x)+(x-1)g'(x)) +H(g(x)+(x+1)g'(x))]-2\left(\frac{\bar{k}_\parallel\bar{U}_{z0}}{\gamma_0}\right)(A+B)h(x) +2\left(\frac{\bar{k}_\parallel\bar{U}_{z0}}{\gamma_0}\right)\left[\frac{2}{\bar{\omega}}\left(\frac{mJ_m}{\bar{k}_\perp\bar{r}_0}\right)+(x+1)A+(x-1)B\right]h'(x) +\left(\frac{\bar{k}_\parallel\bar{U}_{z0}}{\gamma_0}\right)^2\left(\frac{\gamma_0}{\bar{\Omega}}\right)\left[\frac{2}{\bar{\omega}}\left(\frac{mJ_m}{\bar{k}_\perp\bar{r}_0}\right) +(x^++1)A+(x^+-1)B\right]h(x^-) -\left(\frac{\bar{k}_\parallel\bar{U}_{z0}}{\gamma_0}\right)^2\left(\frac{\gamma_0}{\bar{\Omega}}\right)\left[\frac{2}{\bar{\omega}}\left(\frac{mJ_m}{\bar{k}_\perp\bar{r}_0}\right) +(x^-+1)A+(x^--1)B\right]h(x^+)\right\} \tag{61}$$

$$a_5 = -\left(\frac{1}{4\gamma_0}\right)\left(\frac{\gamma_0}{\bar{\Omega}}\right)(J_m'')\left(\frac{\bar{k}_\perp \bar{U}_{\perp 0}}{\bar{k}_\parallel \bar{U}_{z0}}\right)\left(\frac{\bar{k}_\parallel \bar{U}_{z0}}{\gamma_0}\right)^2$$
$$\cdot\left\{2\left[A\frac{\left((\psi^+)^2-\left(\frac{\bar{\Omega}}{\gamma_0}\right)^2\right)}{\psi^+\frac{\bar{\Omega}}{\gamma_0}}+B\frac{\left((\psi^-)^2-\left(\frac{\Omega}{\gamma_0}\right)^2\right)}{\psi^-\frac{\bar{\Omega}}{\gamma_0}}\right.\right.$$
$$\left.+\frac{2}{\bar{\omega}}\left(\frac{mJ_m}{\bar{k}_\perp \bar{r}_0}\right)\left(\frac{\bar{k}_\parallel \bar{U}_{z0}}{\gamma_0}\right)\frac{\gamma_0}{\bar{\Omega}}\right]h(x)$$
$$-\left[A\left(\frac{\gamma_0}{\bar{\Omega}}\right)\left(\psi^+ + \frac{\bar{\Omega}}{\gamma_0}\right)+B\left(\frac{\gamma_0}{\bar{\Omega}}\right)\left(\psi^- + \frac{\bar{\Omega}}{\gamma_0}\right)\right.$$
$$+\frac{2}{\bar{\omega}}\left(\frac{mJ_m}{\bar{k}_\perp \bar{r}_0}\right)\left(\frac{\bar{k}\|\bar{U}_{z0}}{\gamma_0}\right)\frac{\gamma_0}{\bar{\Omega}}\Big]h(x^-)-\Big[A\left(\frac{\gamma_0}{\bar{\Omega}}\right)\left(\psi^+ - \frac{\bar{\Omega}}{\gamma_0}\right)$$
$$\left.\left.+B\left(\frac{\gamma_0}{\bar{\Omega}}\right)\left(\psi^- - \frac{\bar{\Omega}}{\gamma_0}\right)+\frac{2}{\bar{\omega}}\left(\frac{mJ_m}{\bar{k}_\perp \bar{r}_0}\right)\left(\frac{\bar{k}\|U_{z0}}{\gamma_0}\right)\frac{\gamma_0}{\bar{\Omega}}\right]h(x^+)\right\} \tag{62}$$

where

$$x = \frac{\left(\frac{m\bar{\Omega}}{\gamma_0}-\bar{\omega}\right)}{\left(\frac{\bar{k}_\parallel \bar{U}_{z0}}{\gamma_0}\right)} \tag{63}$$

$$x^\pm = \frac{\left((m\pm 1)\frac{\bar{\Omega}}{\gamma_0}-\bar{\omega}\right)}{\left(\frac{\bar{k}_\parallel \bar{U}_{z0}}{\gamma_0}\right)} \tag{64}$$

$$g(x) = \left[\frac{\cos\left(\frac{\pi l x}{2}+\frac{\pi}{2}(l-1)\right)}{(x^2-1)}\right]^2 \tag{65}$$

and

$$h(x) = (x^2-1)g(x). \tag{66}$$

Using (57), $\eta/\bar{E}_0^2$ is plotted as a function of magnetic field in Fig. 2 for several values of γ_0 for a typical cavity operating in the TE_{511} mode. The central mth harmonic emission-absorption feature, as well as the $(m-1)$th harmonic emission and the $(m+1)$th harmonic absorption features, are evident. The $(m-1)$th harmonic feature lies at higher $\bar{B}_0$, and the $(m+1)$th harmonic feature lies at lower $\bar{B}_0$ relative to the mth harmonic feature. In Fig. 3 is shown the dependence of $\eta/\bar{E}_0^2$ on the axial mode number l for TE_{51l}. When $l=1$, there is a single mth harmonic emission peak due to cross-coupling between the forward and backward waves. For larger l, the interactions occur primarily for two magnetic-field values. For long cavities, large $\bar{L}$, $\bar{\omega} \simeq \bar{k}_\perp$, and the peaks occur at $m\bar{\Omega}/\gamma_0 \simeq \bar{k}_\perp \pm \bar{k}_\parallel \beta_{\parallel 0}$. These emission peaks are displaced to either side of the $l=1$ peak. For short cavities, small $\bar{L}$, the increase in $\bar{\omega}$ with increasing $\bar{k}_\parallel$ causes both peaks to be shifted to higher $\bar{B}_0$.

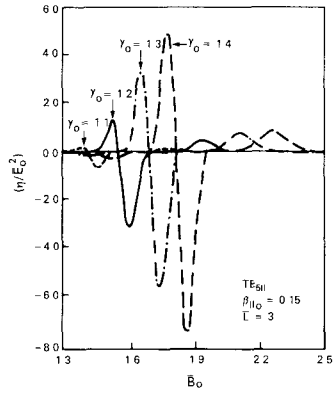

Fig. 2. Efficiency as a function of $\bar{B}_0$ for several values of γ_0.

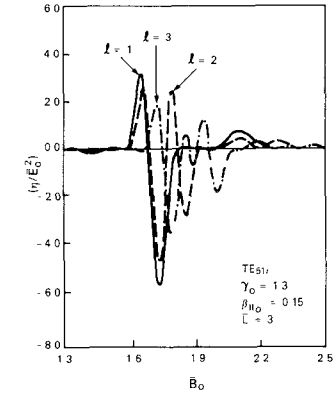

Fig. 3. Efficiency as a function of $\bar{B}_0$ for TE_{51l}.

At the mth harmonic, three separate interactions exist. For fast-wave systems with $\bar{U}_{\perp 0}/\gamma_0 \simeq 1$ and $\bar{U}_{\parallel 0}/\gamma_0 \ll 1$, the dominant interaction comes from azimuthal bunching due to the relativistic mass cyclotron maser effect, and is contained in term a_4 ($\delta\theta$ coupled to $\bar{E}_\theta$). Strong emission or absorption is present, depending upon whether $m\Omega/\gamma_0 \lesssim \omega$ or $m\Omega/\gamma_0 \gtrsim \omega$, respectively. Axial magnetic bunching, the Weibel-type instability, also occurs, and is contained in term a_3 ($\delta\bar{z}$ coupled to $\bar{E}_\theta$), but is small for the fast wave (see Chu and Hirshfield [35]). For $l=1$, axial bunching leads to an enhancement of the cyclotron maser emission due to cross-coupling between the forward and backward waves. At large l numbers, the cross-coupling decreases, and axial bunching detracts from the cyclotron maser emission (this is detraction grows with increasing l due to the increased RF magnetic field). A third interaction also takes place, causing absorption. This instability comes from the tendency of those electrons which gain energy to spiral outwards to regions of stronger fields which enhance the energy gain, and for those electrons which lose energy

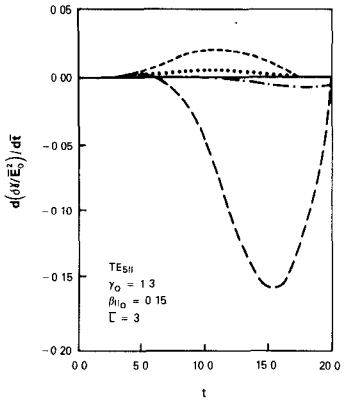

Fig. 4. Variation of $d(\delta\gamma/\bar{E}_0^2)/d\bar{t}$ as a function of $\bar{t}$ for TE_{511}. The separate terms shown come from: $\delta(\bar{U}_l/\gamma)\bar{E}_r$ [——], $\delta(\bar{U}_\theta/\gamma)\bar{E}_\theta$ [· · · ·], $\delta\theta(\partial\bar{E}_\theta/\partial\theta)$ [— —], $\delta z(\partial E_\theta/\partial\bar{z})$ [· · ·], $\delta\bar{r}(\partial\bar{E}_\theta/\partial\bar{r})$ [----].

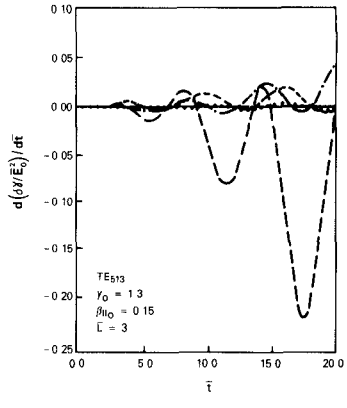

Fig. 5. Variation of $d(\delta\gamma/\bar{E}_0^2)/d\bar{t}$ as a function of $\bar{t}$ for TE_{513}. The separate terms shown come from: $\delta(\bar{U}_r/\gamma)\bar{E}_r$ [——], $\delta(\bar{U}_\theta/\gamma)\bar{E}_\theta$ [· · · ·], $\delta\theta(\partial\bar{E}_\theta/\partial\theta)$ [— —], $\delta z(\partial E_\theta/\partial\bar{z})$ [· · ·], $\delta\bar{r}(\partial\bar{E}_\theta/\partial\bar{r})$ [----].

to spiral inwards to regions of weaker fields (e.f., McDermott *et al.* [41]). This absorption instability is contained in both terms a_5 ($\delta\bar{r}$ coupled to $\bar{E}_\theta$) and in a_4.

At the $(m-1)$th and $(m+1)$th harmonics, there is a single dominant instability. This interaction is nonrelativistic in nature, and is due to a combinations of $\boldsymbol{E}\times\boldsymbol{B}$ and $\nabla\boldsymbol{B}\times\boldsymbol{B}$ drifts in terms a_2, a_4, and a_5. At the $(m-1)$th harmonic, the shift leads to emission, while at the $(m+1)$th harmonic it causes absorption.

The time derivative of $\delta\gamma/\bar{E}_0^2$ as a function of transit time between $\bar{z}=0$ and $\bar{z}=\bar{L}$ is shown in Figs. 4 and 5. These figures correspond to the cases of maximum $\eta/\bar{E}_0^2$ for $l=1$ and $l=3$ shown in Fig. 3. The $l=1$ case involves forward and backward wave interaction. The $l=3$ case is dominated by resonant interaction with the forward wave. The dominance of the cyclotron maser emission term is evident in both, as is the switch from weak emission to strong absorption for the axial-bunching term. The radial term leads to absorption for both $l=1$ and $l=3$.

We can accurately approximate $\delta\gamma$ near the mth harmonic for $\bar{\omega}\gg\bar{k}_\parallel$ and $\beta_{\parallel 0}\ll 1$ as

$$\delta\gamma\simeq\left(\frac{\bar{E}_0}{\bar{k}_\parallel\beta_{\parallel 0}}\right)^2\left(\frac{J_m'(\bar{k}_\perp\bar{r}_0)}{\gamma_0}\right)\cdot\left[2\left(\beta_{\perp 0}mJ_m''(\bar{k}_\perp\bar{r}_0)+J_m'(\bar{k}_\perp\bar{r}_0)\right)g(x)-\beta_{\perp 0}^2\left(\frac{\bar{\omega}}{\bar{k}_\parallel\beta_{\parallel 0}}\right)J_m'(\bar{k}_\perp\bar{r}_0)g'(x)\right]. \quad (67)$$

The magnetic mistuning for the cyclotron maser emission peak occurs at $x\lesssim -1$ for $l=1$, and $x\lesssim\pm 1$ for $l>1$. The RF field here rotates slightly faster than the electrons, and "catches" the bunched particles in a phase where they lose energy. The maximum values of g and g' are $g=1$ for $l=1$, $g\sim\frac{1}{2}l^2$ for $l>1$, and $g'\sim l^3/2$, for all l. Cyclotron maser emission will remain strong, as long as

$$\left(\frac{\bar{L}\bar{\omega}}{2\pi\beta_{\parallel 0}}\right)\left[\frac{\beta_{\perp 0}^2J_m'(\bar{k}_\perp\bar{r}_0)}{\beta_{\perp 0}mJ_m''(\bar{k}_\perp\bar{r}_0)+J_m'(\bar{k}_\perp\bar{r}_0)}\right]\gg 1. \quad (68)$$

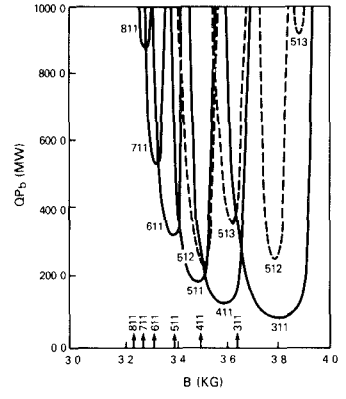

Fig. 6 Start-oscillation beam power for $\gamma_0=1.3$, $\beta_{\perp 10}=0.15$, $\bar{L}=3$. Arrows give optimum operating magnetic-field values.

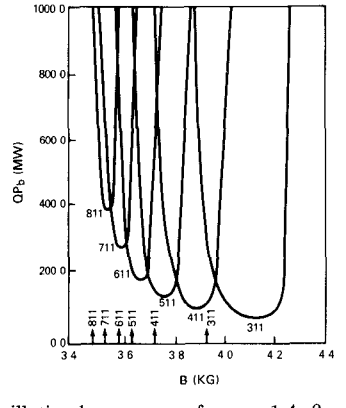

Fig. 7. Start-oscillation beam power for $\gamma_0=1.4$, $\beta_{\parallel 0}=0.15$, and $\bar{L}=3$. Arrows give optimum operating magnetic-field values.

In this limit, η near the emission peak is

$$\eta\simeq\frac{(\bar{E}_0)^2}{2(\gamma_0-1)}\left(\frac{\bar{\omega}}{\gamma_0}\right)\left(\frac{\bar{L}}{\pi\beta_{\parallel 0}}\right)^3(\beta_{\perp 0})^2\left[J_m'(\bar{k}_\perp\bar{r}_0)\right]^2. \quad (69)$$

Using the full linear theory for efficiency, as stated in (57), we have calculated the start-oscillation condition. Using (19), the power balance requirement for oscillation is shown in Figs. 6 and 7, which contain graphs of QP_b versus B_0, the applied magnetic field. These figures show the

mode overlap between the mth harmonic resonances for TE_{m11} modes with $m = 3$–8. The increase of QP_b with m comes primarily from the decrease in $J_m'(\bar{k}_\perp \bar{r}_0)$. The resonance widths narrow as $1/m$ with increasing m. TE_{mn1} modes with $n > 1$ also emit strongly at the mth harmonic, but at much higher frequencies and magnetic fields. For small n, the start-oscillation beam power is nearly the same as for the TE_{m11} modes. We have shown in Fig. 6 the $l = 1$, 2, and 3 longitudinal modes for TE_{51l}. When $\bar{L} = 3$, increasing the l number leads to the generation of two resonances, both of which are shifted to higher magnetic fields. The increase in start-oscillation power with increasing l is due to the detrimental effects of axial bunching. When $\bar{L}$ is larger, one resonance peak of the $l > 1$ modes may overlap with the next-higher TE_{m11} mode, leading to mode competition [41]. This form of mode overlap can be suppressed by use of cavity designs for which Q decreases rapidly with l the axial mode number [3] (see [53] for a discussion of axial mode competition). The relation for minimum start-oscillation beam power can be found by combining (19) and (69) and is given by

$$QP_b(\min) \simeq \frac{3\times 10^7(\beta_{\parallel 0})^3\gamma_0(\gamma_0-1)(J_m(x_{mn}))^2(1-m^2/x_{mn}^2)}{(\bar{L})^2(\beta_{\perp 0})^2(J_m'(\beta_{\perp 0}m))^2}\ \text{kW}. \tag{70}$$

IV. Nonlinear Regime

For large-amplitude RF fields in the nonlinear regime, we have solved for the particle dynamics numerically, using (9)–(15). Taking advantage of the m-fold RF-field symmetry for TE_{mnl} modes and the fact that a circularly polarized field simply rotates with time, an axially symmetric electron beam can be modeled by injecting electrons equally spaced in the injection angle between $\theta = 0$ and $\theta = 2\pi/m$ at $\bar{z} = 0$, $\bar{t} = 0$. The symmetries are lost for off-axis beams, and here the test electrons, at $\bar{t} = 0$, were placed equally spaced in θ over 2π and equally in $\bar{z}$ over the distance $2\pi\beta_{\parallel 0}/\bar{\omega}$ just outside the cavity to account for temporal phase effects. Between 50–100 particles were used with a resulting error of $\leqslant 1$ percent in the computed efficiency. The numerical results give excellent agreement for weak fields compared with the linear calculations. Efficiencies were calculated by following the test electron orbits through the gyrotron cavity until they exited, and then using the energy loss averaged over the test electron population.

In the high-field regime, we are concerned largely with maximum efficiencies as a function of beam and cavity parameters. Efficiencies are optimized by searching over the cavity field amplitude $\bar{E}_0$ and the external magnetic field $\bar{B}_0$ until the maximum was found. The limitation on the efficiency when $\bar{\omega} \gg \bar{k}_\parallel$, $\beta_{\parallel 0} \ll 1$, $\beta_{\perp 0} \simeq 1$ is due to phase trapping of the electrons [17], [36]. Fig. 8 shows phase plots for a typical case as a function of $\bar{z}$ along the cavity. Electrons lose energy when the phase $m\theta - \bar{\omega}\bar{t}$ is between 0 and π and gain energy between π and 2π. The

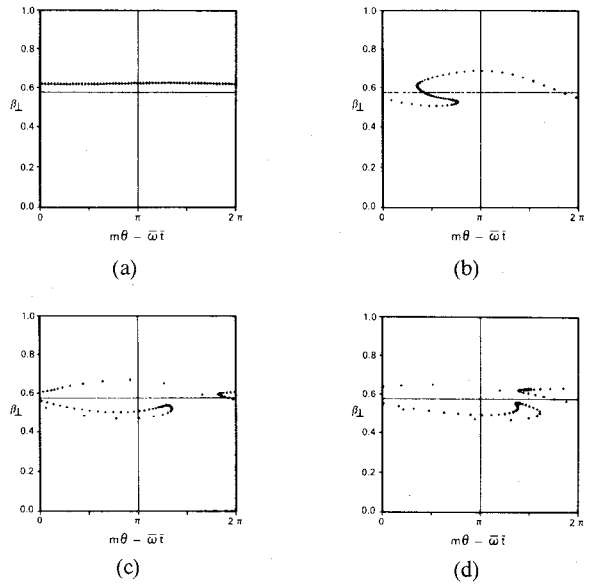

Fig. 8. Phase plots as a function of $\bar{z}$ for TE_{m11}, $\beta_{110} = 0.15$, $\gamma_0 = 1.3$, $\bar{L} = 3$, $\bar{E} = 0.66$, $\bar{B}_0 = 1.59$. The value of $\bar{z}$ is for each graph (a) 0.2, (b) 1.6, (c) 2.4, and (d) 3.

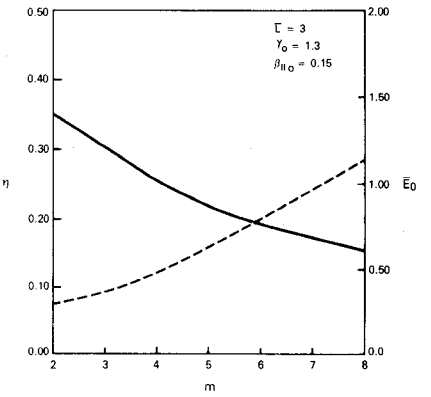

Fig. 9. Optimum efficiency [——] and corresponding value of $\bar{E}_0$ [----] as a function of m for TE_{m11} modes.

horizontal line gives the value of $\beta_\perp$ for electron co-rotation with the field. Particles which lose energy tend to perform counter-clockwise orbits about the intersection of the crossed lines in the figures. Maximum efficiency occurs for values of $\bar{E}_0$ and $\bar{B}_0$, such that the electrons are bunched in phase between 0 and π near $\bar{L}/2$, where the RF electric field is strongest. The electrons may thereafter move into the energy-gaining phase regime, but by then the electric-field amplitude has greatly diminished.

We have studied the dependence of the maximum efficiency on a number of parameters. Figs. 9–12 show the variation as a function of m, γ_0, $\beta_{\parallel 0}$, and $\bar{L}$ for axis-encircling beams ($\bar{r}_{gc} = 0$). The efficiency decreases with increasing m number for TE_{m11} modes as shown in Fig. 9. For large m, the decay goes roughly as $1/m$. This behavior appears to be due to the increasing difficulty to obtain phase bunching in the RF-field azimuthal lobes. Since $d\delta\theta/d\bar{t} \simeq -\bar{\Omega}\delta\gamma/\gamma_0^2$ and the lobes θ extent decreases as $1/m$, it is not surprising that the average optimized $\delta\gamma$ also should vary as $1/m$.

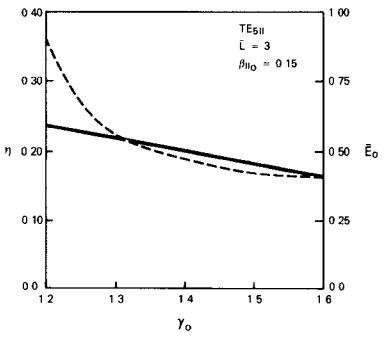

Fig. 10. Optimum efficiency [——] and corresponding value of $\bar{E}_0$ [---] as a function of γ_0, for fixed $\beta_{\|0}$.

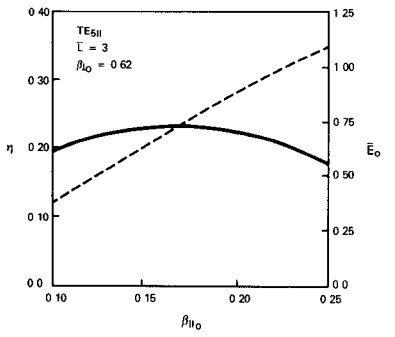

Fig. 11. Optimum efficiency [——] and corresponding value of $\bar{E}_0$ [---] as a function of $\beta_{\|0}$, for fixed $\beta_{\perp 0}$.

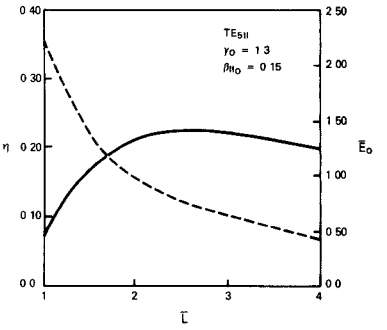

Fig. 12. Optimum efficiency [——] and corresponding value of $\bar{E}_0$ [---] as a function of $\bar{L}$.

The optimum efficiency is a weakly varying function of γ_0, $\beta_{\|0}$, and $\bar{L}$ for $\bar{\omega} \gg \bar{k}_{\|}$. For small $\bar{L}$, however, axial bunching competes with the cyclotron maser emission process and η is greatly reduced. Outside of this regime, the effects of varying γ_0, $\beta_{\|0}$, or $\bar{L}$ can be countered by adjusting $\bar{E}_0$ and $\bar{B}_0$. For $\beta_{\perp 0} \simeq 1$, we find the approximate relation

$$\bar{E}_0 \propto \frac{\beta_{\|0}}{\bar{L}} \left[J_m' \left(\frac{x_{mn} \bar{U}_{\perp 0}}{\bar{B}_0} \right) \right]^{-1} \tag{71}$$

holds over a wide range of parameters. This simply is a statement that, for optimum efficiency, the electric field times the transit time is nearly constant. While our results show that high efficiencies are possible for low γ_0 beams, the large start-oscillation beam powers needed for them at the high m harmonics make their use impractical.

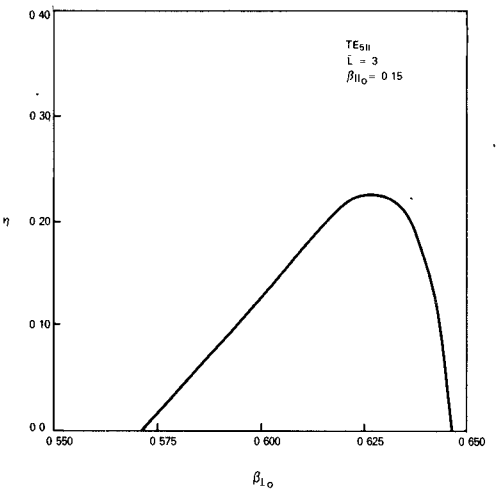

Fig. 13. Variation in efficiency about the optimum as a function of $\beta_{\perp 0}$, with fixed $\bar{E}_0 = 0.66$, $\bar{B}_0 = 1.59$.

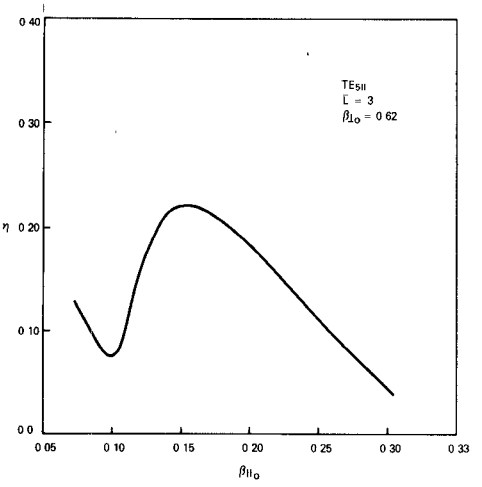

Fig. 14. Variation in efficiency about the optimum as a function of $\beta_{\|0}$, with fixed $\bar{E}_0 = 0.66$, $B_0 = 1.59$.

Actual electron beams are never without some velocity spread. We have investigated the effects of velocity spread on the efficiency by taking a TE_{511} system optimized for $\gamma_0 = 1.3$, $\beta_{\|0} = 0.15$, and calculating the dependence of η upon $\beta_{\perp 0}$ and $\beta_{\|0}$ at fixed RF-field values. These calculations show that the variations in η has a full width at half the maximum efficiency of ~ 0.05 for $\beta_{\perp 0}$ and ~ 0.14 for $\beta_{\|0}$. In Figs. 13 and 14, the profiles are given for η versus $\beta_{\perp 0}$ and η versus $\beta_{\|0}$. The peak efficiency in both figures corresponds to the optimized values. The $\beta_{\perp 0}$ full-width at half the optimum efficiency corresponds to a variation in γ_0 of ~ 5 percent, which is comparable to the average γ variation itself which takes place during energy loss at peak efficiency. Velocity spreads in $\beta_{\perp 0}$ causing γ_0 variations of $\leqslant 2.5$ percent about the optimum γ_0 should lead to net efficiencies greater than half of the optimum value. η is much less sensitive to variations in $\beta_{\|0}$. A spread of 10 percent in $\beta_{\|0}$ here would lead to net efficiencies ~ 90 percent of the optimum.

From the start-oscillation beam power curves in Figs. 6 and 7, it appears that the optimum efficiency may be hard

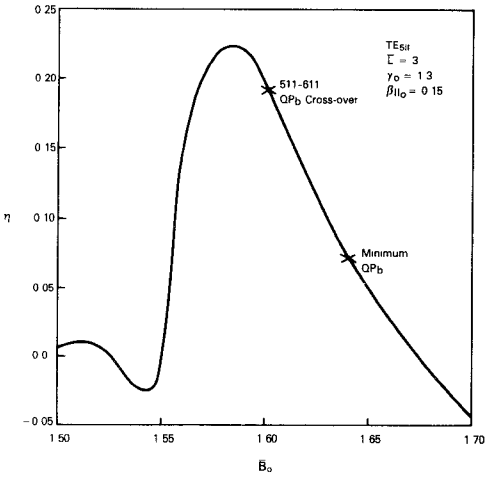

Fig. 15. Efficiency as a function of $\bar{B}_0$ about the optimum $\bar{E}_0 = 0.66$, $\bar{B}_0 = 1.59$ peak.

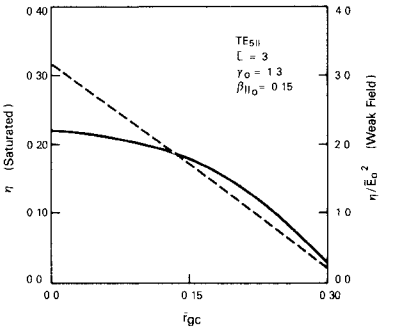

Fig. 16. Efficiency as a function of off-axis guiding center displacement for an optimized [——] TE_{511} efficiency at $\bar{E}_0 = 0.66$, $\bar{B}_0 = 1.59$ and for the weak-field [---] efficiency at the start-oscillation minimum beam power $\bar{B}_0 = 1.62$.

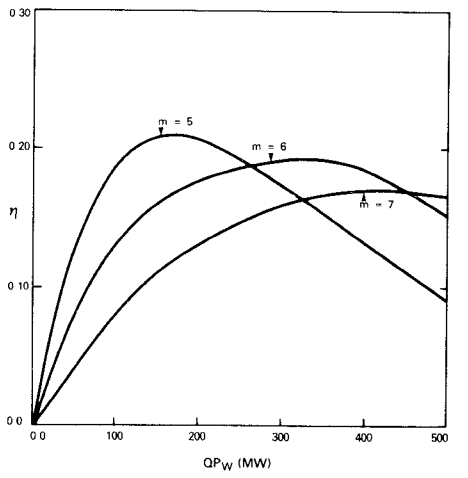

Fig. 17. Efficiency as a function of cavity radiation losses QP_w for $\gamma_0 = 1.3$, $\beta_{\|0} = 0.15$, $\bar{L} = 3$, $m = 5$, 6, and 7. The values of $\bar{B}_0$ for $m = 5$, 6, and 7 are, respectively, $\bar{B}_0 = 1.60$, 1.56, and 1.54, and correspond to start-oscillation beam powers which are just below the next-higher mode.

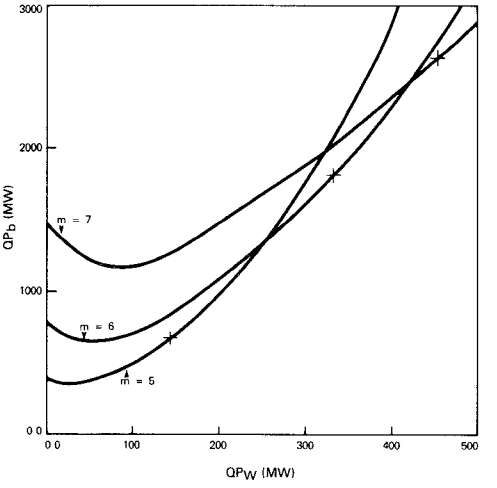

Fig. 18. Beam-power requirements QP_b as a function of QP_w for the parameters in Fig. 17. The crosses mark the point of maximum efficiency for each m.

to achieve due to mode competition. The arrows in these figures show the optimum efficiency magnetic-field values. In steady-state operation, one may, however, start off with beam or magnetic-field parameters, such as to start off a particular mode and thereafter adjust the system [7], [37] either raising γ_0 or lowering $\bar{B}_0$ until one is operating in the optimum regime. This cannot be done, though, for pulsed systems whose field decays between bursts. The competition problem is not really severe, though. If one looks at η plotted as a function of $\bar{B}_0$ at optimum $\bar{E}_0$ (see, for example, Fig. 15 for the TE_{511} case) the peak is broad enough to allow near-optimum efficiencies well out of the competition region. In fact, for the case treated in Fig. 15, if one adjusts $\bar{E}_0$ about the TE_{511}–TE_{611}-mode QP_b cross-over point, an efficiency of 21 percent can be reached (optimum efficiency is 22 percent for this case). The beam may also be prebunched as in a gyroklystron amplifier [54], in order to bias a given mode and reduce mode competition.

One may worry also about the effect of beam placement upon the efficiency. We have considered the dependence of η upon the guiding center location for TE_{511} in two cases. The first is in the weak-field regime where $\bar{B}_0$ is set at the minimum-beam power value, and the second is for optimal $\bar{B}_0$, $\bar{E}_0$. The results are shown in Fig. 16. Displacement of the guiding center up to 15 percent of $\bar{r}_w$ (30 percent of the Larmor radius) produces little effect upon the saturated efficiency. The start-oscillation value, though, appears to decrease linearly with $\bar{r}_{gc}$. A 10-percent displacement would lead here to a 20-percent increase in start-oscillation beam power.

As a final result, we present efficiencies and beam powers QP_b as a function of cavity-radiated power QP_w for $m = 5$, 6, and 7 for a $\gamma_0 = 1.3$, $\beta_{\|0} = 0.15$, $\bar{L} = 3$ gyrotron (see Figs. 17 and 18). The values of $\bar{B}_0$ chosen correspond to start-oscillation beam powers, which are just slightly lower for the mode in question than for the next-higher mode. The start-oscillation power (QP_b value when $QP_w = 0$) can be reduced by increasing γ_0 or $\bar{L}$, or by decreasing $\beta_{\|0}$. The value of $\bar{E}_0$, and hence QP_w, at optimum efficiency would be decreased, also. We have seen that η in the saturated regime would be weakly affected by these changes.

V. Conclusions

We have presented here a linear and nonlinear analysis of the TE_{m11} whispering-gallery-mode gyrotron. Analytic solutions for the weak-field efficiency and start-oscillation beam power are given. We find that resonances occur at the mth and $(m \pm 1)$th cyclotron harmonics. The mth harmonic interaction leads to emission from the cyclotron maser instability. The $(m+1)$th and $(m-1)$th resonances give, respectively, absorption and emission due to a radial instability. Our analysis shows that large efficiency may be generated for the mth harmonic interaction, $\geqslant 35$ percent, using high-energy beams, and that optimal efficiencies can be quite insensitive to beam and cavity conditions over a broad range of parameters. With an increasing m number, however, the maximum efficiency was found to decrease. Our calculations were made for fixed-background fields. It has been shown that tapered magnetic fields and tapered cavities can lead to enhanced efficiencies [36], [37], and this should be looked into for TE_{m11} mode systems. Higher efficiencies may also be obtainable through the $(m-1)$th harmonic interaction, which does not involve bunching due to the relativistic mass effect in conventional gyrotrons.

References

[1] V. A. Flyagin, A. V. Gaponov, M. I. Petelin, and V. K. Yulpatov, "The gyrotron," *IEEE Trans. Microwave Theory Tech.*, vol. MTT-25, pp. 514–521, 1977.

[2] J. L. Hirshfield and V. L. Granatstein, "The electron cyclotron maser-An historical survey," *IEEE Trans. Microwave Theory Tech.*, vol. MTT-25, pp. 522–527, 1977.

[3] A. V. Gaponov, V. A. Flyagin, A. L. Gol'denberg, G. S. Nusinovich, Sh. E. Tsimring, V. G. Usov, and S. N. Vlasov, "Powerful millimetre-wave gyrotrons," *Int. J. Electron.*, vol. 51, pp. 277–302, 1981.

[4] P. A. Lindsay, "Gyrotrons (electron cyclotron masers): Different mathematical models," *IEEE J. Quantum Electron.*, vol. QE-17, pp. 1327–1333, 1981.

[5] R. S. Symons and H. R. Jory, "Cyclotron resonance devices," *Advances in Electronics and Electron Physics*, vol. 55, L. Marton and C. Marton, eds. New York: Academic Press, 1981, pp. 1–75.

[6] V. L. Granatstein, M. Read, and L. R. Barnett, "Measured performance of gyrotron oscillators and amplifiers," *Int. J. Infra. Mill. Waves*, vol. 5, 1982.

[7] K. J. Kim, M. E. Read, J. M. Baird, K. R. Chu, A. Drobot, J. L. Vomvoridis, A. Ganguly, D. Dialetis, and V. L. Granatstein, "Design considerations for a megawatt CW gyrotron," *Int. J. Electron.*, vol. 51, pp. 427–445, 1981.

[8] V. V. Alikaev, G. A. Bobrovskii, V. I. Poznyak, K. A. Razumova, V. V. Sannikov, Yu. A. Sokolov, and A. A. Shmarin, "ECR plasma heating in the TM-3 Tokamak in magnetic fields up to 25 kOe," *Fiz. Plazmy*, vol. 2, pp. 390–395, 1976; also in *Sov. J. Plasma Phys.*, vol. 2, pp. 212–215, 1976.

[9] R. M. Gilgenbach, M. E. Read, K. E. Hackett, R. Lucey, B. Hui, V. L. Granatstein, K. R. Chu, A. C. England, C. M. Loring, O. C. Eldridge, H. C. Howe, A. G. Kulchar, E. Lazarus, M. Murakami, and J. B. Wilgen, "Heating at the electron cyclotron frequency in the ISX-B tokamak," *Phys. Rev. Lett.*, vol. 44, pp. 647–650, 1980.

[10] S A. Freije, K. W. Arnold, and R. H. Whitney, "Impact of gyrotron characteristics on a mirror reactor," *Int. J. Electron*, vol. 53, pp. 595–604, 1982.

[11] L. R. Wicker and D. C. Webb, "The potential military applications of millimeter waves," in *North Atlantic Treaty Organization AGARD Conf. Proc. No. 245*, p. 1, Munich, W. Ger., Sept 1982.

[12] A. V. Gaponov and V. K. Yulpatov, "Interaction of helical electron beams with the electromagnetic field in a waveguide," *Radio Eng. Electron. Phys.*, vol. 12, pp. 582–587, 1967.

[13] Yu. V. Bykov, A. V. Gaponov, and M. J. Petelin, "On the theory of a traveling-wave cyclotron-resonance maser (CRM) amplifier with a transverse electron stream," *Radio Phys. Quantum Electron*, vol 17, pp. 928–931, 1974.

[14] E. Ott and W. M. Manheimer, "Theory of microwave emission by velocity-space instabilities of an intense relativistic electron beam," *IEEE Trans. Plasma Sci.*, vol. PS-3, pp. 1–5, 1975.

[15] P. Sprangle and W. M. Manheimer, "Coherent nonlinear theory of a cyclotron instability," *Phys. Fluids*, vol. 18, pp. 224–230, 1975.

[16] P. Sprangle, "Excitation of electromagnetic waves from a rotating annular relativistic e-beam," *J. Appl. Phys.*, vol. 47, pp. 2935–2940, 1976.

[17] P. Sprangle and A. T. Drobot, "The linear and self-consistent nonlinear theory of the electron cyclotron maser instability," *IEEE Trans. Microwave Theory Tech.*, vol. MTT-25, pp. 528–544, 1977.

[18] K. R. Chu, A. T. Drobot, V. L. Granatstein, J. L. Seftor, "Characteristics and optimum operating parameters of a gyrotron traveling wave amplifier," *IEEE Trans. Microwave Theory Tech.*, vol. MTT-27, pp. 178–187, 1979.

[19] B. Etlicher, A. Huetz, J. M. Buzzi, P. Haldenwang, and D. Legueau, "Microwave generation by intense relativistic electron beams propagating in a circular waveguide," *J. App. Phys.*, vol. 51, pp. 61–67, 1980.

[20] K. R. Chu and A. T. Drobot, "Theory and single wave simulation of the gyrotron traveling wave amplifier operating at cyclotron harmonics," NRL Memo. Rep. 3788, 1978.

[21] P. A. Lindsay, R. J. Lumsden, and R. M. Jones, "A dispersive equation for gyrotron TWTs," *Int. J. Electron.*, vol. 53, pp. 619–640, 1982.

[22] A. K. Ganguly and S. Ahn, "Self-consistent large signal theory of the gyrotron traveling wave amplifier," *Int. J. Electron.*, vol. 53, pp. 641–658, 1982.

[23] M. Caplan, A. T. Lin, and K. R. Chu, "A study of the saturated output of a TE_{01} gyrotron using an electromagnetic finite size particle code," *Int. J. Electron.*, vol. 53, pp. 659–672, 1982.

[24] J. L. Hirshfield, I. B. Bernstein, and J. M. Wachtel, "Cyclotron resonance interaction of microwaves with energetic electrons," *IEEE J. Quantum Electron.*, vol. QE-1, pp. 237–245, 1965.

[25] T. W. Hsu and P. N. Robinson, "Negative absorption from weakly relativistic electrons traversing a Cuccia coupler," *Electron Lett.*, vol. 1, pp. 84–85, June 1965.

[26] A. V. Gaponov, M. I. Petelin, and V. K. Yulpatov, "The induced radiation of excited classical oscillators and its use in high-frequency electronics," *Radio Physics and Quantum Electron.*, vol. 10, pp. 794–813, 1967.

[27] G. N. Rapoport, A. K. Nemak, and V. A. Zhurakhovskiy, "Interaction between helical electron beams and strong electromagnetic cavity-fields at cyclotron frequency harmonics," *Radio Eng. Electron Phys.*, vol. 12, pp. 587–595, 1967.

[28] A. F. Kurin, "Cyclotron maser theory," *Radio Eng. Electron. Phys.*, vol. 14, pp. 1652–1654, 1969.

[29] B. Kulke, "Limitations on millimeter-wave power generation with spiraling electron beams," *IEEE Trans. Electron Devices*, vol. ED-19, pp. 71–79, 1972.

[30] S. V. Kolosov and A. A. Kurayev, "Comparative analysis of the interaction at the first and second harmonics of the cyclotron frequency in gyroresonance devices," *Radio Eng. Electron. Phys.*, vol. 19, pp. 65–73, 1974.

[31] A. A. Kurayev, F. G. Schevchenko, and V. P. Shestakovich, "Efficiently optimized output cavity profiles that provide a higher margin of gyroklystron stability," *Radio Eng. Electron. Phys.*, vol. 19, pp. 96–103, 1974.

[32] V. L. Bratman and A. E. Tokarev, "On the theory of the relativistic cyclotron-resonance maser," *Izv. Vyssh. Ucheb. Zaved. Radio-fiz.*, vol. 17, p. 1224, 1974; also in *Radio Phys. Quantum Electron.*, vol. 17, pp. 932–935, 1974.

[33] M. I. Petelin and V. K. Yulpatov, "Linear theory of a monotron cyclotron-resonance maser," *Radio Phys. Quantum Electron.*, vol. 18, pp. 212–219, 1975.

[34] K R. Chu, "Theory of electron cyclotron maser interaction in a cavity at the harmonic-frequencies," *Phys. Fluids*, vol. 21, pp. 2354–2364, 1978.

[35] K. R. Chu and J. L. Hirshfield, "Comparative study of the axial and azimuthal bunching mechanisms in electromagnetic cyclotron instabilities," *Phys. Fluids*, vol. 21, pp. 461–466, 1978.

[36] P. Sprangle and R. A. Smith, "The nonlinear theory of efficiency enhancement in the electron cyclotron maser," *J. Appl. Phys.*, vol. 51, pp. 3001–3007, 1980.

[37] K. R. Chu, M. E Read, and A. K. Ganguly, "Methods of efficiency enhancement and scaling for the gyrotron oscillator," *IEEE Trans. Microwave Theory Tech.*, vol. MTT-28, pp. 318–325, 1980.

[38] A. W. Fliflet, M. E. Read, K. R. Chu, and R. Seeley, "A self-consistent field theory for gyrotron oscillators: application to a low Q gyromonotron," *Int. J. Electron.*, vol. 53, pp. 505–552, 1982.
[39] Y. Y. Lau and L. R. Barnett, "Theory of a low magnetic field gyrotron-gyromagnetron," *Int. J. Infra. Mill. Waves*, vol. 3, pp. 619–644, 1982.
[40] Y. Y. Lau and L. R. Barnett, "A low magnetic field gyrotron-gyromagnetron," *Int. J. Electron.*, vol. 53, pp. 693–698, 1982.
[41] D. B. McDermott, N. C. Luhmann, Jr., and A. Kupiszewski, "Small-signal theory of a large-orbit electron-cyclotron harmonic maser," *Phys. Fl.*, vol. 26, pp. 1936–1941, 1983.
[42] A. F. Kurin, "Linear theory of the cyclotron maser," *Radio Phys. Quantum Electron.*, vol. 10, pp. 651–654, 1967.
[43] A. F. Kurin, G. A. Kurina, V. V. Nivokov, "Nonlinear theory for a cyclotron-resonance maser with a Fabry-Perot resonator," *Radio Phys. Quantum Electron.*, vol. 19, pp. 742–747, 1976.
[44] P. Sprangle, W. M. Manheimer, and J. L. Vomvoridis, "Theory of the quasioptical electron cyclotron maser," *Phys. Rev. A.*, vol. 23, pp. 3127–3138, 1981.
[45] J. L. Vomvoridis, "Self-consistent non-linear analysis of overmoded gyrotron oscillators," *Int. J. Infra. Mill. Waves*, vol. 3, pp. 339–366, 1982.
[46] A. Bondeson, B. Levush, V. M. Manheimer, and E. Ott, "Multimode theory and simulation of quasioptical gyrotrons and gyroklystrons," *Int. J. Electron.*, vol. 53, pp. 547–553, 1982.
[47] H. R. Jory, "Investigation of electronic interactions with optical resonators for microwave generation and applications," U.S. Army Electron. Research and Development Tech. Rep. ECOM-01873-F, 1968.
[48] W. W. Destler, R. L. Weiler, and C. D. Strittler, "High power microwave wave generation from a rotating e layer in a magnetron-type waveguide," *Appl. Phys. Lett.*, vol. 38, pp. 570–572, 1981.
[49] H. R. Jory and A. W. Trivelpiece, "Charged-particle motion in a large-amplitude electromagnetic fields," *J. Appl. Phys.*, vol. 39, pp. 3053–3060, 1968.
[50] W. Miner, P. Vitello, and A. T. Drobot, "Theory and numerical simulation of a TE_{111} gyroresonant accelerator," to be published.
[51] D. B. McDermott, N. C. Luhmann, Jr., D. S. Furuno, and A. Kupiszewski, "Operation of a millimeter-wave harmonic gyrotron," *Int. J. Infra. Mill. Waves*, to be published.
[52] G. Dohler, "Peniotron interactions in gyrotrons (II: Quantitative Analysis)," preprint 1983.
[53] K. W. Kreischer and R. J. Temkin, "Mode excitation in a gyrotron operating at the fundamental," *Int. J. Infra. Mill. Waves*, vol. 2, pp. 175–196, 1981.
[54] A. K. Ganguly and K. R. Chu, "Analysis of a two-cavity gyroklystron," *Int. J. Electron.*, vol. 51, pp. 503–520, 1981.

✤

Peter Vitello was born in Glendale, CA on September 15, 1950. He received the B.S. degree in physics in 1972 from the University of Southern California, Los Angeles, CA, and the Ph.D. degree in theoretical physics in 1977 from Cornell University, Ithaca, NY.

He is a member of the Plasma Physics Division at Science Applications, Inc., McLean, VA. He is currently working on high-harmonic gyrotron oscillators and gyroklystron amplifiers.

Dr. Vitello is a member of the American Physical Society and of the American Astronomical Society.

✤

William H. Miner, Jr., was born in Jacksonville, NC, on August 27, 1949. He received the B.A. degree in physics from Rollins College, Winter Park, FL, in 1971, and the Ph.D. degree in physics from the University of Texas at Austin in 1978.

He is a member of the Technological Systems Group at Science Applications, Inc., McLean, VA. He is a research physicist and is currently involved in analytical and numerical investigations of microwave generation and diode physics. In the area of microwave generation, he is studying the physics of compact, high-harmonic gyrotrons. He is also investigating the stability of electron flow in planar diodes.

Dr. Miner is a member of the American Physical Society.

✤

Adam T. Drobot was born in Zakopane, Poland, on May 13, 1947. He received the B.S. degree in engineering physics from Cornell University, Ithaca, NY, in 1968, and the Ph.D. degree in physics from the University of Texas at Austin in 1974.

He has been working at Science Applications, Inc., McLean, VA, on the application of numerical and computational techniques to the simulation of complex physical systems involving the interaction of electromagnetic fields with high-density energetic particles. He has contributed recently to work on: collective ion acceleration, free-electron lasers, and the basic theory and simulation of high-power microwave sources such as gryotrons, magnetrons, and klystrons. He currently is involved in problems of power flow in high-power magnetically insulated transmission lines, and in intense relativistic diodes. He is the manager of the Plasma Physics Division in the Technological Systems Group at Science Applications, Inc.

Dr. Drobot is a member of the American Physical Society, Sigma Phi Sigma, and Phi Kappa Phi.